# CMS Physics Analysis Summary

Contact: cms-pag-conveners-heavyions@cern.ch 2019/11/06

# Studies of charm and beauty long-range correlations in pp and pPb collisions

The CMS Collaboration

## Abstract

Studies of collective long-range (large $\eta$ gap) correlations involving open charm and beauty hadrons in pp and pPb collisions are presented, using data samples collected by the CMS experiment with center-of-mass energies of 13 and 8.16 TeV, respectively. The elliptic flow harmonics ($v_2$) of prompt and nonprompt $D^0$ mesons (from beauty hadron decays) are extracted from long-range two-particle azimuthal correlations, with respect to inclusive charged particles. In pp collisions, positive $v_2$ signals for prompt charm hadrons are reported for the first time over a transverse momentum ($p_{\mathrm{T}}$) range of 2-4 GeV. The signals are comparable to those for light-flavor hadron species. Compared at similar event multiplicities, the prompt $D^0$ meson $v_2$ values in pp and pPb are similar in magnitude. The $v_2$ signal for open beauty hadrons is extracted for the first time via nonprompt $D^0$ meson in pPb collisions, with a magnitude smaller than that for prompt $D^0$ meson at $p_{\mathrm{T}}$ between 2-5 GeV. The new measurements provide strong indications of a postive charm hadron $v_2$ in the smallest pp systems and a flavor hierarchy of $v_2$ between charm and beauty hadrons in the pPb systems, providing key insights to further understand the origin of heavy flavor quark collectivity in small-system collisions.

# 1 Introduction

Strong collective behavior, particularly observed in the azimuthal correlations of particles emitted over a wide pseudorapidity range, in high-energy nucleus-nucleus (AA) collisions at the BNL RHIC [1–4] and the CERN LHC [5–10], has indicated the formation of a hot, strongly interacting quark-gluon plasma (QGP) matter, which exhibits nearly ideal hydrodynamic behavior [11–13]. Although not originally expected, similar long-range collective azimuthal correlations are also observed in recent years for small systems with high final-state particle multiplicity such as proton-proton (pp) [14–18], proton-nucleus (pA) [19–28], and lighter nucleus-nucleus systems [28–31], while there is no observation of long-range correlations in $e^+e^-$ collisions [32], which raised the question of whether a tiny fluid-like QGP medium with a significantly smaller size is created there[33]. In the context of hydrodynamic models, the observed azimuthal correlation structure of emitted particles is typically characterized by its Fourier components [34]. The second and third Fourier anisotropy coefficients are known as elliptic ($v_2$) and triangular ($v_3$) flow. These coefficients most directly reflect the QGP medium response to the initial collision geometry and its fluctuations [35–38]. While experimental measurements in these small systems are consistent with the dominance of strong final-state interactions such as a hydrodynamic expansion of a tiny QGP droplet, alternative scenarios based on gluon saturation in the initial state can also capture the main features of the correlation data, and are conjectured to play a dominant role as the event multiplicity decreases [33, 39].

Due to the large masses, heavy flavor quarks (charm and bottom) are produced in the very early stages of the hadronic collision via hard scatterings. They are available to probe both initial- and final-state effects of the collision dynamics [40, 41]. In AA collisions, a strong elliptic flow signal of open heavy flavor $D^0$ mesons is observed in both AuAu collisions at RHIC [42] and PbPb collisions at the LHC [43–45], which suggests that charm quarks develop strong collective behavior via strong interactions with the bulk of the QGP medium. Measurements of elliptic flow of hidden charm mesons, $J/\psi$, provide further evidence for strong rescatterings of charm quarks and their subsequent collectivity developed in the deconfined QGP medium [46, 47].

In small systems the study of heavy flavor hadron collectivity has the potential of providing key insights to disentangle possible contributions from both initial- and final-state effects. In particular, heavy flavor hadrons may be more sensitive to possible initial-state gluon saturation effects. Recent observation of a significant elliptic flow signal for prompt $D^0$ [48] and prompt $J/\psi$ [49, 50] mesons in pPb collisions provided the first strong evidence for charm quark collectivity in small systems. Surprisingly, the observed $v_2$ signal for prompt $J/\psi$ meson in pPb collisions is found to be comparable to that of prompt $D^0$ mesons and light flavor hadrons at a given particle transverse momentum ($p_T$). This behavior cannot be explained by the final-state effects of a QGP medium alone [51], and may suggest the existence of initial-state correlation effects [52]. Further detailed investigations are important to address many open questions in understanding the origin of heavy flavor quark collectivity in small systems, including its multiplicity dependence in both pPb and pp systems, and its collective behavior of beauty and charm quarks.

This PAS presents the first measurement of the elliptic flow ($v_2$) for prompt $D^0$ mesons in pp collisions at $\sqrt{s}$ = 13 TeV and for nonprompt $D^0$ mesons (from decays of beauty hadrons) in pPb collisions at $\sqrt{s_{NN}}$ = 8.16 TeV, using long-range two-particle angular correlations. The $v_2$ harmonic is determined over a wide $p_T$ range from 2–8 GeV for prompt $D^0$ mesons as a function of multiplicity, comparing pp and pPb collision systems. The nonprompt $D^0$ mesons $v_2$ is extracted in high-multiplicity pPb collisions, for $2 < p_T < 5$ GeV and $5 < p_T < 8$ GeV, and is compared to previous measurements of prompt $D^0$ mesons and light flavor hadrons.

## 2 Experimental apparatus and data sample

The central feature of the CMS apparatus is a superconducting solenoid of 6 m internal diameter, providing a magnetic field of 3.8 T. Within the solenoid volume, there are four primary subdetectors including a silicon pixel and strip tracker detector, a lead tungstate crystal electromagnetic calorimeter, and a brass and scintillator hadron calorimeter, each composed of a barrel and two endcap sections. Iron and quartz-fiber Cherenkov hadron forward calorimeters cover the range $2.9 < |\eta| < 5.2$. Muons are measured in gas-ionization detectors embedded in the steel flux-return yoke outside the solenoid. The silicon tracker measures charged particles within the range $|\eta| < 2.5$. For charged particles with $1 < p_{\mathrm{T}} < 10\,\mathrm{GeV}$ and $|\eta| < 1.4$, the track resolutions are typically 1.5% in $p_{\mathrm{T}}$ and 25–90 (45–150) $\mu$m in the transverse (longitudinal) impact parameter [53]. A detailed description of the CMS detector, together with a definition of the coordinate system used and the relevant kinematic variables, can be found in Ref. [54].

The pPb data at $\sqrt{s_{_{NN}}} = 8.16\,\mathrm{TeV}$ used in this analysis were collected by the CMS experiment in 2016, and correspond to an integrated luminosity of $186\,\mathrm{nb}^{-1}$ [55]. The beam energies are 6.5 TeV for the protons and 2.56 TeV per nucleon for the lead nuclei. Because of the asymmetric beam conditions, particles selected in this analysis from midrapidity in the laboratory frame ($|y_{\mathrm{lab}}| < 1$) correspond to rapidity in the nucleon-nucleon center-of-mass frame of $-1.46 < y_{\mathrm{cm}} < 0.54$, with positive rapidity corresponding to the proton beam direction. The pp data at $\sqrt{s} = 13\,\mathrm{TeV}$ were collected in 2017 and 2018 with integrated luminosity of $1.27\,\mathrm{pb}^{-1}$ [56] and $10.22\,\mathrm{pb}^{-1}$ [57] during special runs with low beam intensity, resulting in an average number of concurrent pp collisions of about 1 per bunch crossing. The event reconstruction, event selections, and triggers (minimum-bias trigger and high multiplicity trigger) are identical to those described in Refs. [17, 58, 59]. Similar to previous CMS correlation measurements, the pPb and pp data are analyzed for several multiplicity ($N_{\mathrm{trk}}^{\mathrm{offline}}$) classes, where $N_{\mathrm{trk}}^{\mathrm{offline}}$ is the number of primary tracks [53] with $|\eta_{\mathrm{lab}}| < 2.4$ and $p_{\mathrm{T}} > 0.4\,\mathrm{GeV}$.

## 3 Prompt and nonprompt $\mathrm{D}^0$ reconstruction and selection

The $\mathrm{D}^0$ (and its charge conjugate state) mesons are reconstructed through the hadronic decay channel $\mathrm{D}^0 \to K^- \pi^+$. In order to suppress the combinatorial background and improve the momentum and mass resolution, high-purity [53] tracks with $p_{\mathrm{T}} > 0.7\,\mathrm{GeV}$, $|\eta_{\mathrm{lab}}| < 2.4$ and relative error on $p_{\mathrm{T}} < 10\%$ are used. For each pair of selected tracks, two $\mathrm{D}^0$ candidates are considered by assuming one of the tracks has the pion mass while the other track has the kaon mass, and vice versa.

The $\mathrm{D}^0$ candidates are selected according to their daughter charged particle track kinematics, numbers of valid hits and relative $p_{\mathrm{T}}$ uncertainties, the $\chi^2$ probability of both daughter tracks to originate from a common decay vertex, the three-dimensional distance (with and without being normalized by its uncertainty) between the primary and decay vertices, and the pointing angle (defined as the angle between the line segment connecting the primary and decay vertices and the momentum vector of the reconstructed particle candidates in the plane transverse to the beam direction). The selection is optimized separately for pp and pPb results as well as each individual $p_{\mathrm{T}}$ range, using a multivariate technique that employs the boosted decision tree (BDT) algorithm [60], in order to maximize the statistical significance of the prompt or nonprompt $\mathrm{D}^0$ meson signals. The signal samples are taken from simulated samples of PYTHIA 8.209 [61] tune CUETP8M1 [62]. (embedded into EPOS LHC [63] for the case of pPb analysis) for both prompt and nonprompt $\mathrm{D}^0$ events. The background samples for the multivariate training are taken from data. In the BDT training for prompt $\mathrm{D}^0$ signals, same-charge sign can-

didates are used, which contain predominantly combinatorial backgrounds. For optimizing nonprompt $D^0$ signals, both prompt $D^0$ signals and combinatorial candidates are considered dominant backgrounds to be suppressed. For this reason, opposite-charge sign candidates (although including small fractions (<5%) of nonprompt $D^0$ signals) are used for the background training sample. This approach is found to give better performance than using same-charge sign background candidates in achieving higher nonprompt $D^0$ fractions, especially at higher $p_T$.

The optimal selection criterion is the working point with the highest signal significance of prompt and nonprompt $D^0$ signals, respectively. In extracting the nonprompt $D^0$ yield, the distributions of distance of closest approach (DCA) of $D^0$ total momentum vector to the primary vertex are fitted, using the template probability distribution functions (PDF) for prompt and nonprompt $D^0$ signals derived from MC simulations. The residual nonprompt fraction in the BDT prompt-trained sample is found to be no more than 7%, while in the BDT nonprompt-trained sample, the optimal selection yields a nonprompt fraction up to 20%. This procedure is further outlined in Sec. 4.

# 4 Analysis

The azimuthal anisotropies of $D^0$ mesons and strange hadrons are extracted from their long-range ($|\Delta\eta| > 1$) two-particle azimuthal correlations with charged particles, as described in Refs. [17, 24]. Taking the $D^0$ meson as an example, the two-dimensional (2D) correlation function is constructed by pairing each $D^0$ candidate with reference primary charged-particle tracks with $0.3 < p_T < 3.0\,\text{GeV}$ (denoted "ref" particles), and calculating

$$\frac{1}{N_{D^0}}\frac{d^2N^{\text{pair}}}{d\Delta\eta\, d\Delta\phi} = B(0,0)\,\frac{S(\Delta\eta,\Delta\phi)}{B(\Delta\eta,\Delta\phi)}, \tag{1}$$

where $\Delta\eta$ and $\Delta\phi$ are the differences in $\eta_{\text{lab}}$ and $\phi$ of each pair. The same-event pair distribution, $S(\Delta\eta,\Delta\phi)$, represents the yield of particle pairs normalized by the number of $D^0$ candidates ($N_{D^0}$) from the same event. The mixed-event pair yield distribution, $B(\Delta\eta,\Delta\phi)$, is constructed by pairing $D^0$ candidates in each event with the reference primary charged-particle tracks from 10 different randomly selected events, from the same $N_{\text{trk}}^{\text{offline}}$ range, and with a primary vertex falling in the same 2 cm wide range of reconstructed $z$ coordinates. The $B(0,0)$ represents the value of $B(\Delta\eta,\Delta\phi)$ at $\Delta\eta = 0$ and $\Delta\phi = 0$. It is evaluated by interpolating the four nearest bins with a bin width of 0.3 in $\Delta\eta$ and $1/16\pi$ in $\Delta\phi$ bilinearly. The interpolation shows negligible effect on the measurements. The analysis procedure is performed in each $D^0$ candidate $p_T$ range by dividing it into intervals of invariant mass. The correction for acceptance and efficiency (derived from simulations using PYTHIA for pp and PYTHIA+EPOS for pPb) of the $D^0$ meson yield is found to have negligible effect on the measurements, and thus is not applied. The $\Delta\phi$ correlation functions averaged over $|\Delta\eta| > 1$ (to remove short-range correlations such as jet fragmentation) is then obtained from the projection of 2D correlation functions and fitted by the first three terms of a Fourier series:

$$\frac{1}{N_{D^0}}\frac{dN^{\text{pair}}}{d\Delta\phi} = \frac{N_{\text{assoc}}}{2\pi}\left[1 + \sum_{n=1}^{3} 2V_{n\Delta}\cos(n\Delta\phi)\right]. \tag{2}$$

Here, $V_{n\Delta}$ are the Fourier coefficients and $N_{\text{assoc}}$ represents the total number of pairs per $D^0$ candidate. Including additional Fourier terms has a negligible effect. By assuming $V_{n\Delta}$ to be the product of single-particle anisotropies [64], $V_{n\Delta}(D^0,\text{ref}) = v_n(D^0)v_n(\text{ref})$, the $v_n$ anisotropy harmonics for $D^0$ candidates can be extracted from the equation:

$$v_n(\mathrm{D}^0) = V_{n\Delta}(\mathrm{D}^0, \mathrm{ref}) / \sqrt{V_{n\Delta}(\mathrm{ref}, \mathrm{ref})}. \quad (3)$$

Because of limited statistical precision, only the elliptic anisotropy harmonic results are reported in this analysis.

To extract the $V_{2\Delta}$ values of the inclusive $\mathrm{D}^0$ meson signal ($V_{2\Delta}^S$), a two-step fit to the invariant mass spectrum of $\mathrm{D}^0$ candidates and their $V_{2\Delta}$ as a function of the invariant mass, $V_{2\Delta}^{S+B}(m_{\mathrm{inv}})$, is performed in each $p_{\mathrm{T}}$ interval. The mass spectrum fit function is composed of five components: the sum of two Gaussian functions with the same mean but different widths for the $\mathrm{D}^0$ signal, $S(m_{\mathrm{inv}})$; an additional Gaussian function to describe the invariant mass shape of $\mathrm{D}^0$ candidates with an incorrect mass assignment from the exchange of the pion and kaon designations, $SW(m_{\mathrm{inv}})$; crystal ball functions to describe processes $\mathrm{D}^0 \to \pi^+\pi^-$ and $\mathrm{D}^0 \to \mathrm{K}^+\mathrm{K}^-$, $S(m_{\mathrm{K}^+\mathrm{K}^-})$ and $S(m_{\pi^+\pi^-})$; and a third-order polynomial to model the combinatorial background, $B(m_{\mathrm{inv}})$. The contributions from the processes $\mathrm{D}^0 \to \pi^+\pi^-$ and $\mathrm{D}^0 \to \mathrm{K}^+\mathrm{K}^-$ are due to mislabelling K as $\pi$, or vice versa. These two components are emulated by two crystal ball functions at two sides away from the peak region. The width and the ratio of the yields of $SW(m_{\mathrm{inv}})$ and $S(m_{\mathrm{inv}})$ and the crystal ball shape are fixed according to results obtained from simulation studies using PYTHIA for pp collisions and PYTHIA+EPOS for pPb collisions.

The $V_{2\Delta}^{S+B}(m_{\mathrm{inv}})$ distribution is fit with

$$V_{2\Delta}^{S+B}(m_{inv}) = \alpha(m_{inv})\ V_{2\Delta}^{signal} + [1 - \alpha(m_{inv})]\ V_{2\Delta}^{Bkg}(m_{inv}) \quad (4)$$

where

$$\alpha(m_{\mathrm{inv}}) = \frac{S(m_{\mathrm{inv}}) + SW(m_{\mathrm{inv}}) + S(m_{\mathrm{K}^+\mathrm{K}^-}) + S(m_{\pi^+\pi^-})}{S(m_{\mathrm{inv}}) + SW(m_{\mathrm{inv}}) + S(m_{\mathrm{K}^+\mathrm{K}^-}) + S(m_{\pi^+\pi^-}) + B(m_{\mathrm{inv}})}. \quad (5)$$

Here $V_{2\Delta}^B(m_{\mathrm{inv}})$ for the background $\mathrm{D}^0$ candidates is modeled as a linear function of the invariant mass, and $\alpha(m_{\mathrm{inv}})$ is the $\mathrm{D}^0$ signal fraction. The K-$\pi$ swapped, $\mathrm{D}^0 \to \pi^+\pi^-$ and $\mathrm{D}^0 \to \mathrm{K}^+\mathrm{K}^-$ components are included in the signal fraction because these candidates are from genuine $\mathrm{D}^0$ mesons and should have the same $v_2$ value as that of the $\mathrm{D}^0$ signal.

Figure 1 shows an example of fits to the mass spectrum and $V_{2\Delta}^{S+B}(m_{\mathrm{inv}})$, for the BDT prompt-trained sample in the $p_{\mathrm{T}}$ interval 4–6 GeV for the multiplicity range $N_{\mathrm{trk}}^{\mathrm{offline}} \geq 100$ in pp collisions. Similar fits in pPb collisions can be found in Ref. [48], which are not repeated here.

In extracting the $V_{2\Delta}$ values of nonprompt $\mathrm{D}^0$, the measurement and fitting procedure described above are repeated in three separate DCA ranges, containing very different nonprompt $\mathrm{D}^0$ fractions. A linear fit by the functional form,

$$V_{2\Delta}^S = f^{B\to D} V_{2\Delta}^{B\to D} + (1 - f^{B\to D}) V_{2\Delta}^{\mathrm{prompt\ D}}, \quad (6)$$

to the measured $\mathrm{D}^0$ $V_{2\Delta}$ values as a function of nonprompt $\mathrm{D}^0$ fraction is performed to extrapolate to the $V_{2\Delta}$ value at a nonprompt fraction of 100%. The $f^{B\to D}$ represents the nonprompt $\mathrm{D}^0$ fraction. $v_2$ values of nonprompt $\mathrm{D}^0$ are evaluated by using Eq. 3. Figure 2 shows an example of fits to the mass spectrum and $V_{2\Delta}^{S+B}(m_{\mathrm{inv}})$ for the BDT nonprompt-trained sample in DCA$<$0.008 cm and DCA$>$0.0014 cm, in the $p_{\mathrm{T}}$ interval 2–5 GeV for the multiplicity range $185 \leq N_{\mathrm{trk}}^{\mathrm{offline}} < 250$ in pPb collisions. The resulting $\mathrm{D}^0$ signal $V_{2\Delta}$ contains contributions from both prompt and nonprompt $\mathrm{D}^0$ mesons.

Inclusive $\mathrm{D}^0$ meson yields extracted as a function of DCA, by fitting the invariant mass distribution in each DCA bin, are shown in Fig. 3 (left). A template fit to the DCA distribution is

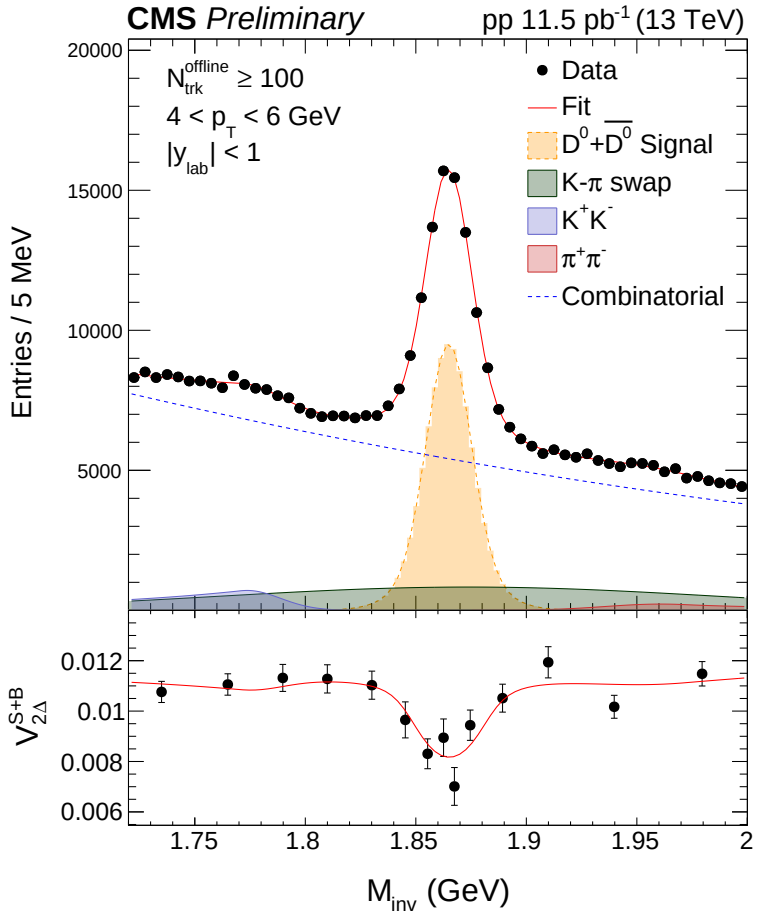


Figure 1: Example of fits to the invariant mass spectrum and $V_{2\Delta}^{S+B}(m_{\mathrm{inv}})$, for the BDT prompt-trained sample in pp collisions.

performed using template distributions of prompt and nonprompt $\mathrm{D}^0$ mesons obtained from MC simulations to constrain the nonprompt $\mathrm{D}^0$ fractions in each of three DCA regions used to extract inclusive $\mathrm{D}^0$ $V_{2\Delta}$, as described above. The inclusive $\mathrm{D}^0$ $V_{2\Delta}$ values from the three DCA regions are then plotted as a function of the corresponding nonprompt $\mathrm{D}^0$ fraction, shown in Fig. 3 (middle and right), for $2 < p_{\mathrm{T}} < 5\,\mathrm{GeV}$ and $5 < p_{\mathrm{T}} < 8\,\mathrm{GeV}$, respectively. The measurements are well described by a linear function fit, which is shown as a red line in Fig. 3.

The residual contribution of back-to-back dijets to the measured $v_2$ results is corrected by subtracting correlations from low-multiplicity events, following an identical procedure established in Refs. [17, 64]. The Fourier coefficients, $V_{n\Delta}$, extracted from Eq. (2) for $N_{\mathrm{trk}}^{\mathrm{offline}} < 35(20)$, in pPb (pp) collisions, are subtracted from the $V_{n\Delta}$ coefficients obtained in the high-multiplicity region, with

$$V_{n\Delta}^{\mathrm{sub}} = V_{n\Delta} - V_{n\Delta}(N_{\mathrm{trk}}^{\mathrm{offline}} < 35)\,\frac{N_{\mathrm{assoc}}(N_{\mathrm{trk}}^{\mathrm{offline}} < 35)}{N_{\mathrm{assoc}}}\,\frac{Y_{\mathrm{jet}}}{Y_{\mathrm{jet}}(N_{\mathrm{trk}}^{\mathrm{offline}} < 35)}. \tag{7}$$

Here, $Y_{\mathrm{jet}}$ represents the jet yield. It is the difference between integrals of the short-range ($|\Delta\eta| < 1$) and long-range ($|\Delta\eta| > 2$) event-normalized associated yields for each multiplicity class. The ratio, $Y_{\mathrm{jet}}/Y_{\mathrm{jet}}(N_{\mathrm{trk}}^{\mathrm{offline}} < 35)$, is introduced to account for the enhanced jet correlations resulting from the selection of higher-multiplicity events. It is observed that the values of jet yield ratio show little dependence on $p_{\mathrm{T}}$ over the full $p_{\mathrm{T}}$ range. For the measurement of

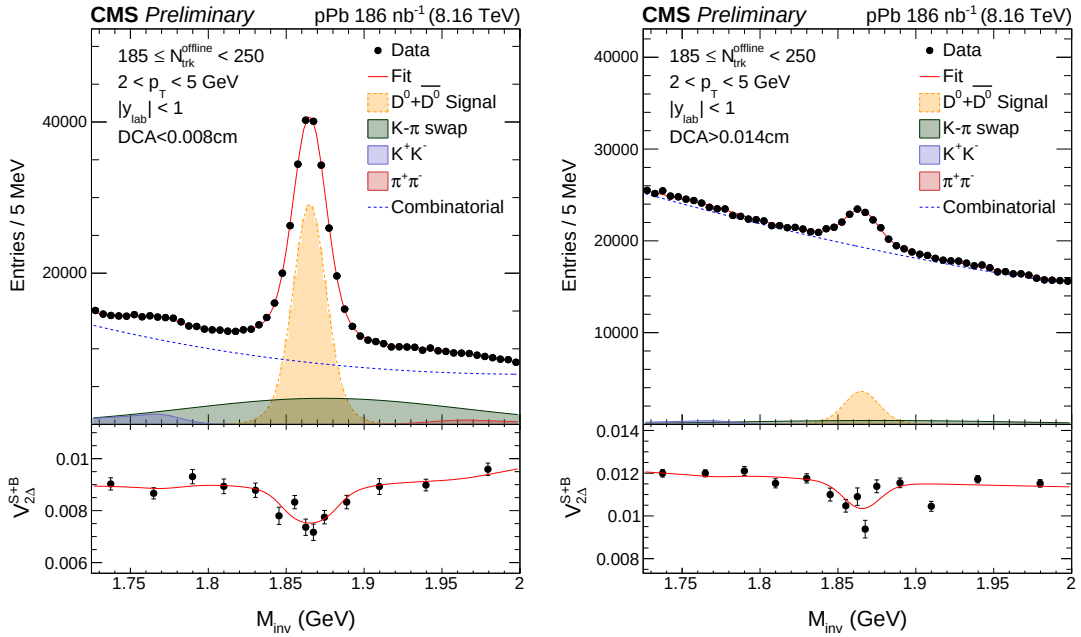


Figure 2: Example of fits to the invariant mass spectrum and $V_{2\Delta}^{S+B}(m_{\mathrm{inv}})$, for the BDT nonprompt-trained sample in pPb collisions. The left shows the fit for DCA<0.008 cm and the right is for DCA>0.014 cm.

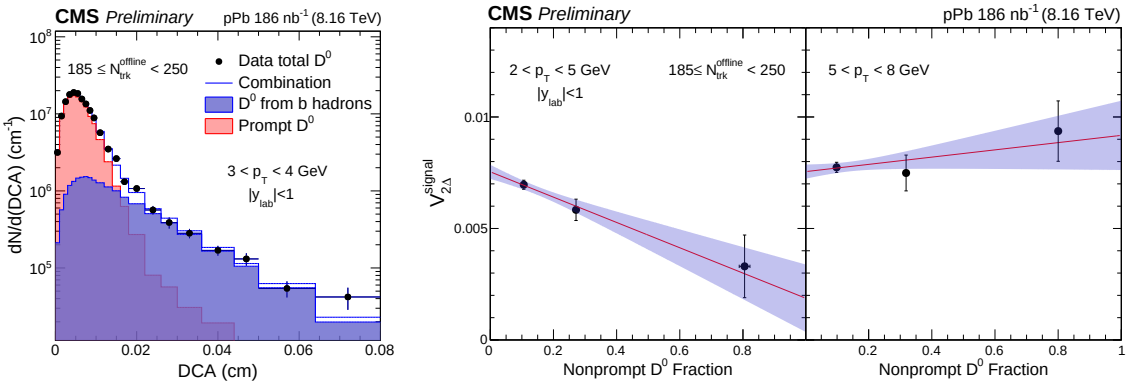


Figure 3: Left: example of template fit to $\mathrm{D}^0$ DCA distribution in the $p_{\mathrm{T}}$ interval 3–4 GeV for events with $185 \leq N_{\mathrm{trk}}^{\mathrm{offline}} < 250$ of pPb collisions. Middle and right: inclusive $\mathrm{D}^0$ $V_{2\Delta}^{signal}$ values from the three DCA regions as a function of the corresponding nonprompt $\mathrm{D}^0$ fraction, for $2 < p_{\mathrm{T}} < 5$ GeV and $5 < p_{\mathrm{T}} < 8$ GeV. The red line is a linear fit to $V_{2\Delta}^{signal}$

nonprompt $\mathrm{D}^0$ mesons, all quantities in Eq. 7 are first extrapolated to values at a nonprompt $\mathrm{D}^0$ fraction of 100%, following the same approach as in Fig. 3 before applying the subtraction procedure.

## 5 Systematic Uncertainties

Systematic uncertainties on the BDT selection and optimization of the $\mathrm{D}^0$ candidates are evaluated by varying the BDT cut value by $\pm 0.05$ around the optimal one to evaluate the stability of the results. This covers the possible difference in the signal BDT distribution between data and MC simulations, which yields a slight difference ($< 0.05$) in the optimal BDT cut value found.

The variations of BDT cut yield the $v_2$ uncertainties of 0.008–0.010 for prompt $D^0$ and 0.032 for nonprompt $D^0$ in pPb collisions. In pp collisions, it brings an uncertainty of 0.003–0.012 on prompt $D^0$ $v_2$.

Other sources of systematic uncertainty include the background mass probability distribution function (PDF), the $D^0$ meson yield correction (acceptance and efficiency correction), and the background $v_2$ PDF. Changing the background mass PDF to a second-order polynomial or an exponential function shows negligible systematic effects. To evaluate the uncertainties arising from the $p_T$-dependent $D^0$ meson yield correction, the $v_2$ values are extracted from the corrected signal $D^0$ distributions and compared to the uncorrected $v_2$ values as a conservative estimate, yielding an uncertainty less than 0.002. The systematic uncertainties from the background $v_2$ PDF are evaluated by changing $v_2^B(m_{\mathrm{inv}})$ to a second-order polynomial function of the invariant mass. It yields an uncertianty less than 0.005. To study potential trigger biases, a comparison to high-multiplicity pPb data for a given multiplicity range that were collected using a lower threshold trigger with 100% efficiency is performed. The uncertainty from trigger bias is quoted as 0.001. The possible contamination by residual pileup interactions is also studied by varying the pileup selection of events in the performed analysis, from no pileup rejection at all to selecting events with only one reconstructed vertex. The variation of $D^0$ $v_2$ values is about 0.002–0.004 in pPb collisions, while it is about 0.004–0.010 in pp collisions due to larger pileup effects.

For the measurement of prompt $D^0$ mesons the contribution from nonprompt $D^0$ mesons is significantly suppressed. No explicit correction is applied and a systematic uncertainty is quoted instead. Based on the prediction for AA collisions that B mesons have a smaller $v_2$ than light-flavor particles, due to the larger mass of the b quark [65–67], the nonprompt $D^0$ $v_2$ values are assumed to lie between 0 and those of strange hadrons. The maximum effect from nonprompt $D^0$ mesons is thus estimated using the extracted nonprompt $D^0$ fraction and the change in $v_2^S$ is found to be smaller than 0.008. For the measurement of nonprompt $D^0$ mesons, a major systematic uncertainty comes from the determination of nonprompt $D^0$ yield fraction in different DCA regions. The DCA template distributions of prompt and nonprompt $D^0$ from MC simulations are smeared to vary the width of DCA distributions and corresponding nonprompt $D^0$ fractions. The variation of DCA width is from 2%–8%, based on the best $\chi^2$ fit to data. The resulting variation in the extracted nonprompt $D^0$ $v_2$ are quoted as a systematic uncertainty, within 0.007.

All sources of systematic uncertainties are added in quadrature to obtain the total systematic uncertainty.

# 6 Results

The elliptic flow ($v_2^{\mathrm{sub}}$) results of prompt $D^0$ mesons in pp collisions at $\sqrt{s} = 13$ TeV are presented in Fig. 4 as a function of $p_T$ for $|y| < 1$, with $N_{\mathrm{trk}}^{\mathrm{offline}} \geq 100$ of high-multiplicity pp collisions at $\sqrt{s} = 13$ TeV. This high-multiplicity region, with $N_{\mathrm{trk}}^{\mathrm{offline}} \geq 100$, hosts approximately $10^{-5}$ of the total inclusive $D^0$ yield. Published data for light-flavor hadrons including inclusive charged particles (dominated by pions), $K_S^0$ and $\Lambda$ are also shown for comparison [17]. Positive $v_2$ signal ($0.061 \pm 0.018(\mathrm{stat.}) \pm 0.014(\mathrm{syst.})$) over a $p_T$ range of ∼2–4 GeV for prompt charm hadrons provides strong indications of the collectivity of charm quarks in pp collisions, with a declining trend toward higher $p_T$. The $v_2$ magnitude for prompt $D^0$ mesons is found to be slightly smaller than that for light-flavor hadron species by about one standard deviation. This is not significant within current experimental uncertainties. The results indicate strong collectivity

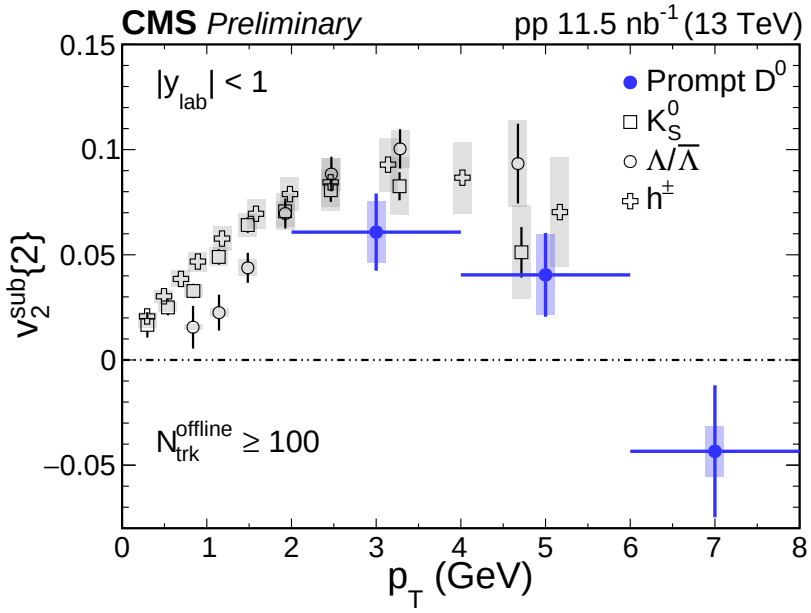


Figure 4: Results of elliptic flow ($v_2^{\rm sub}$) for prompt $\rm D^0$ mesons, as a function of $p_{\rm T}$ for $|y| < 1$, with $N_{\rm trk}^{\rm offline} \geq 100$ in pp collisions at $\sqrt{s} = 13\,\text{TeV}$. Published data for charged particles, $\rm K^0_S$ and $\Lambda$ are also shown for comparison [17]. The error bars correspond to statistical uncertainties, while the shaded areas denote the systematic uncertainties. The horizontal error bars represent the width of the $p_{\rm T}$ bins.

being developed for charm hadrons in pp collisions, which is comparable (or slightly weaker) than that for light-flavor hadrons. This finding is similar to the observation made earlier in pPb collisions over a similar $p_{\rm T}$ range at higher multiplicities $185 \leq N_{\rm trk}^{\rm offline} < 250$ [48].

To further investigate possible system size dependence of collectivity for charm hadrons in small systems, pp and pPb data are directly compared. The prompt $\rm D^0$ $v_2$ as a function of event multiplicity, for three different $p_{\rm T}$ ranges: $2 < p_{\rm T} < 4\,\text{GeV}$, $4 < p_{\rm T} < 6\,\text{GeV}$, and $6 < p_{\rm T} < 8\,\text{GeV}$ are presented in Fig. 5. At similar multiplicities of $N_{\rm trk}^{\rm offline} \sim 100$, the prompt $\rm D^0$ $v_2$ values are found to be comparable within uncertainties in pp and pPb systems. For $2 < p_{\rm T} < 4\,\text{GeV}$, the measured results of prompt $\rm D^0$ provide strong indications of positive $v_2$ down to $N_{\rm trk}^{\rm offline} \sim 50$ with a statistical significance more than 2.5 standard deviation in pPb collisions, while for $6 < p_{\rm T} < 8$ GeV the prompt $\rm D^0$ $v_2$ signal tends to diminish at low multiplicity regions. No clear multiplicity dependence can be determined for pp data, mainly due to large statistical uncertainties at low multiplicities.

The elliptic flow results for nonprompt $\rm D^0$ mesons from beauty hadron decays, corrected for residual jet correlations ($v_2^{\rm sub}$), are shown in Fig. 6 as a function of $p_{\rm T}$ for pPb collisions at 8.16 TeV with $185 \leq N_{\rm trk}^{\rm offline} < 250$. The extracted $v_2^{\rm sub}$ values are $-0.008 \pm 0.028(\text{stat.}) \pm 0.035(\text{syst.})$ for $2 < p_{\rm T} < 5\,\text{GeV}$ and $0.057 \pm 0.029(\text{stat.}) \pm 0.036(\text{syst.})$ for $5 < p_{\rm T} < 8\,\text{GeV}$. At low $p_{\rm T}$, nonprompt $\rm D^0$ $v_2$ is consistent with zero, while at high $p_{\rm T}$, a hint of positive $v_2$ value for beauty mesons is seen but not significant within statistical and systematic uncertainties. Previously published $v_2$ data for prompt $\rm D^0$ mesons and strange hadrons are also shown [48].

At $p_{\rm T} \sim 3$–4 GeV, the nonprompt $\rm D^0$ meson $v_2$ from beauty hadron decays is observed to be smaller than that for prompt $\rm D^0$ mesons with a statistical-only significance of 3.2 standard deviations, strongly suggesting a flavor hierarchy of the collectivity signal that tends to diminish for the heavier beauty hadrons. This finding is qualitatively consistent with the scenario of $v_2$ being generated via final-state rescatterings, where heavier quarks tend to develop a weaker

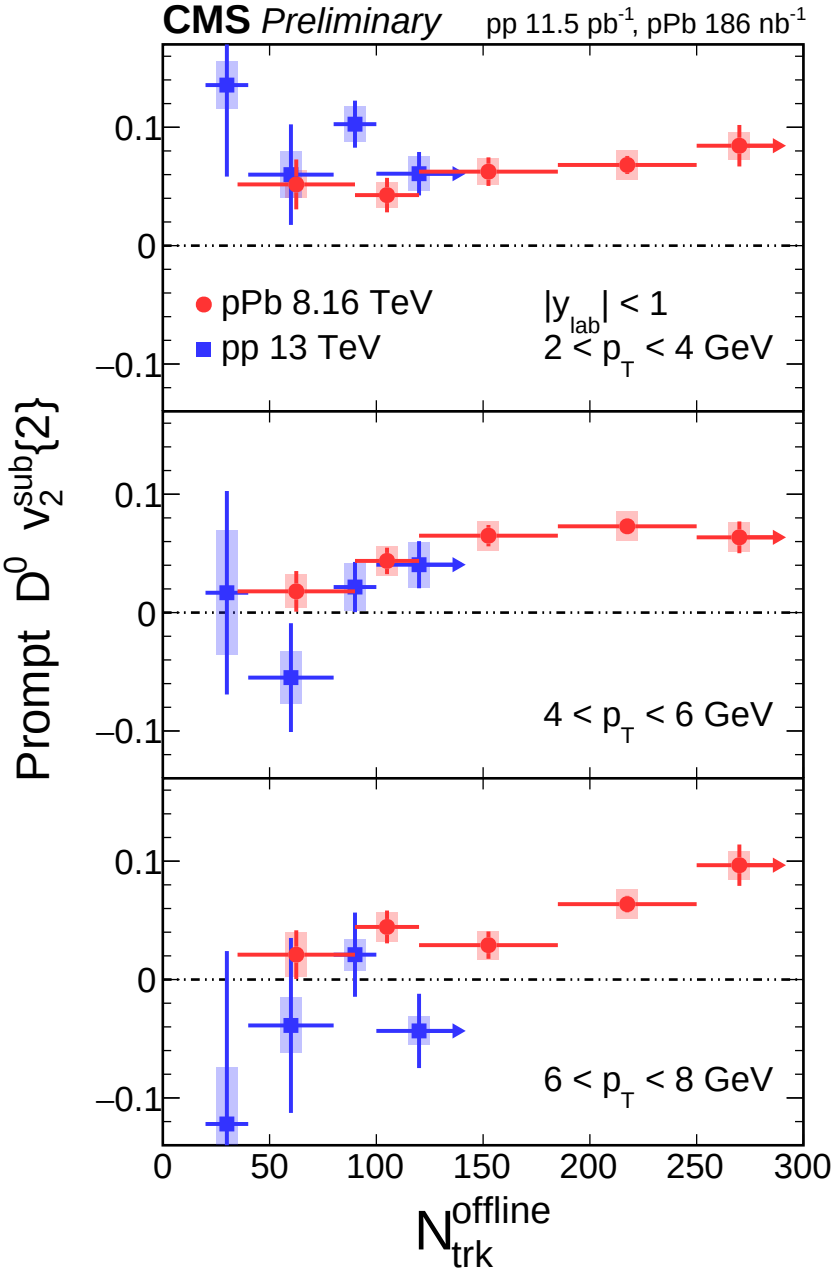


Figure 5: Results of elliptic flow ($v_2^{\mathrm{sub}}$) for prompt $\mathrm{D}^0$ mesons, as a function of event multiplicity for three different $p_{\mathrm{T}}$ ranges, with $|y| < 1$ in pp collisions at $\sqrt{s} = 13\,\mathrm{TeV}$ and pPb collisions at $\sqrt{s_{_{NN}}} = 8.16\,\mathrm{TeV}$. The vertical error bars correspond to statistical uncertainties, while the shaded areas denote the systematic uncertainties. The horizontal error bars represent the width of the $N_{\mathrm{trk}}^{\mathrm{offline}}$ bins. The right-most points with right-arrows correspond to $N_{\mathrm{trk}}^{\mathrm{offline}} \geq 100$ for pp collisions and $N_{\mathrm{trk}}^{\mathrm{offline}} \geq 250$ for pPb collisions.

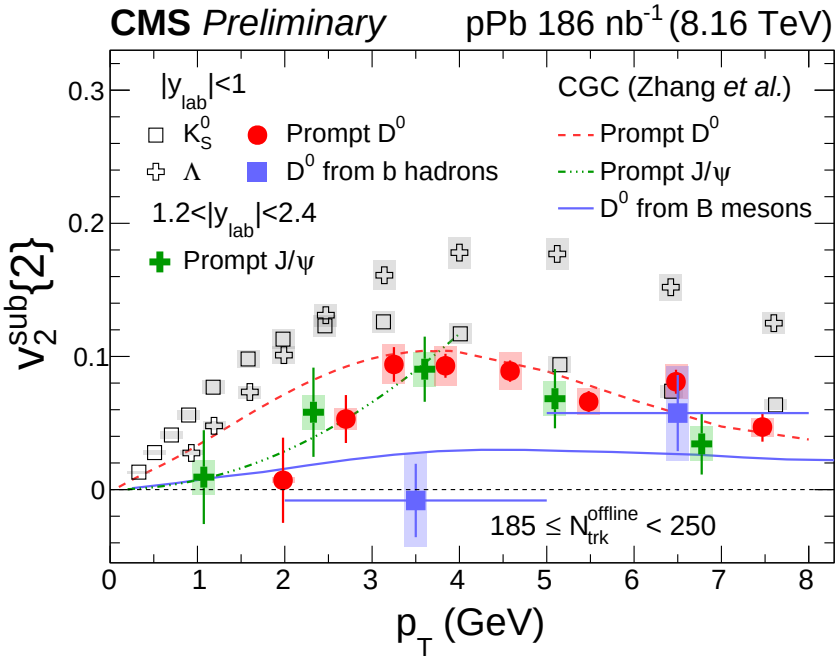


Figure 6: Results of elliptic flow ($v_2^{\rm sub}$) for prompt and nonprompt $\rm D^0$ mesons, as well as $\rm K^0_S$, $\Lambda$ for $|y_{lab}| < 1$, and J/$\psi$ for $1.2 < |y_{lab}| < 2.4$, as functions of $p_{\rm T}$ with $185 \leq N_{\rm trk}^{\rm offline} < 250$ in pPb collisions at $\sqrt{s_{_{NN}}} = 8.16$ TeV[48, 50]. The error bars correspond to statistical uncertainties, while the shaded areas denote the systematic uncertainties. The horizontal error bars represent the width of the nonprompt $\rm D^0$ $p_{\rm T}$ bins. Dash line, dash-dotted line and solid line show the theoretical calculation of prompt $\rm D^0$, J/$\psi$ and nonprompt $\rm D^0$ under color glass condensate (CGC) framework respectively [52].

collective $v_2$ signal. However, as shown in Ref. [50], the observed large $v_2$ signal for prompt J/$\psi$ meson cannot be explained by the model calculation based on final-state interactions between produced charm quarks and a QGP medium, which may indicate the presence of additional contributions such as those from initial-state interactions. Calculations of $v_2$ signals for prompt J/$\psi$, prompt and nonprompt (from B meson decay) $D^0$ mesons from initial-state long-range correlations, based on the color glass condensate framework [52], are compared to data in Fig. 6. A flavor hierarchy between prompt and nonprompt $D^0$ is also strongly suggested, especially at low $p_T$, consistent with experimental evidence within uncertainties.

# 7 Summary

The first measurements of elliptic azimuthal anisotropies for prompt $D^0$ mesons in pp collisions at $\sqrt{s}$ = 13 TeV, and for nonprompt $D^0$ mesons from beauty hadron decays in pPb collisions at $\sqrt{s_{NN}}$ = 8.16 TeV are presented. In pp collisions with $N_{trk}^{offline} \geq 100$, strong indications of positive $v_2$ signals for prompt charm hadrons are reported for the first time over a transverse momentum ($p_T$) range of 2-4 GeV, which is found to be comparable (or slightly smaller) to those for light-flavor hadron species. Compared at similar event multiplicities, the prompt $D^0$ meson $v_2$ values in pp and pPb are found to be similar in magnitude. The $v_2$ signal of open beauty hadrons is extracted for the first time via non-prompt $D^0$ meson in pPb collisions, with a magnitude smaller than that for prompt $D^0$ mesons at $p_T \sim$ 3-4 GeV. The new measurements of charm hadron $v_2$ in the smallest pp system and the strong indications of mass dependence of heavy flavor hadron $v_2$ in the pPb system provide key insights to understand the origin of heavy flavor quark collectivity in small-system collisions.

# References


[1] PHOBOS Collaboration, "System size dependence of cluster properties from two-particle angular correlations in Cu+Cu and Au+Au collisions at $\sqrt{s_{NN}}$ = 200 GeV", *Phys. Rev. C* **81** (2010) 024904, doi:10.1103/PhysRevC.81.024904, arXiv:0812.1172.

[2] STAR Collaboration, "Distributions of charged hadrons associated with high transverse momentum particles in pp and Au + Au collisions at $\sqrt{s_{NN}}$ = 200 GeV", *Phys. Rev. Lett.* **95** (2005) 152301, doi:10.1103/PhysRevLett.95.152301, arXiv:nucl-ex/0501016.

[3] STAR Collaboration, "Long range rapidity correlations and jet production in high energy nuclear collisions", *Phys. Rev. C* **80** (2009) 064912, doi:10.1103/PhysRevC.80.064912, arXiv:0909.0191.

[4] PHOBOS Collaboration, "High transverse momentum triggered correlations over a large pseudorapidity acceptance in Au+Au collisions at $\sqrt{s_{NN}}$ = 200 GeV", *Phys. Rev. Lett.* **104** (2010) 062301, doi:10.1103/PhysRevLett.104.062301, arXiv:0903.2811.

[5] CMS Collaboration, "Long-range and short-range dihadron angular correlations in central PbPb collisions at a nucleon-nucleon center of mass energy of 2.76 TeV", *JHEP* **07** (2011) 076, doi:10.1007/JHEP07(2011)076, arXiv:1105.2438.

[6] CMS Collaboration, "Centrality dependence of dihadron correlations and azimuthal anisotropy harmonics in PbPb collisions at $\sqrt{s_{NN}}$ = 2.76 TeV", *Eur. Phys. J. C* **72** (2012) 2012, doi:10.1140/epjc/s10052-012-2012-3, arXiv:1201.3158.

[7] ALICE Collaboration, "Elliptic flow of charged particles in Pb-Pb collisions at 2.76 TeV", *Phys. Rev. Lett.* **105** (2010) 252302, doi:10.1103/PhysRevLett.105.252302, arXiv:1011.3914.

[8] ATLAS Collaboration, "Measurement of the azimuthal anisotropy for charged particle production in $\sqrt{s_{NN}}$ = 2.76 TeV lead-lead collisions with the ATLAS detector", *Phys. Rev. C* **86** (2012) 014907, doi:10.1103/PhysRevC.86.014907, arXiv:1203.3087.

[9] CMS Collaboration, "Measurement of the elliptic anisotropy of charged particles produced in PbPb collisions at nucleon-nucleon center-of-mass energy = 2.76 TeV", *Phys. Rev. C* **87** (2013) 014902, doi:10.1103/PhysRevC.87.014902, arXiv:1204.1409.

[10] CMS Collaboration, "Studies of azimuthal dihadron correlations in ultra-central PbPb collisions at $\sqrt{s_{NN}}$ = 2.76 TeV", *JHEP* **02** (2014) 088, doi:10.1007/JHEP02(2014)088, arXiv:1312.1845.

[11] J.-Y. Ollitrault, "Anisotropy as a signature of transverse collective flow", *Phys. Rev. D* **46** (1992) 229, doi:10.1103/PhysRevD.46.229.

[12] U. Heinz and R. Snellings, "Collective flow and viscosity in relativistic heavy-ion collisions", *Ann. Rev. Nucl. Part. Sci.* **63** (2013) 123, doi:10.1146/annurev-nucl-102212-170540, arXiv:1301.2826.

[13] C. Gale, S. Jeon, and B. Schenke, "Hydrodynamic Modeling of Heavy-Ion Collisions", *Int. J. Mod. Phys. A* **28** (2013) 1340011, doi:10.1142/S0217751X13400113, arXiv:1301.5893.

[14] CMS Collaboration, "Observation of Long-Range Near-Side Angular Correlations in Proton-Proton Collisions at the LHC", *JHEP* **09** (2010) 091, doi:10.1007/JHEP09(2010)091, arXiv:1009.4122.

[15] ATLAS Collaboration, "Observation of long-range elliptic anisotropies in $\sqrt{s}$ =13 and 2.76 TeV $pp$ collisions with the ATLAS detector", arXiv:1509.04776.

[16] CMS Collaboration, "Measurement of long-range near-side two-particle angular correlations in pp collisions at $\sqrt{s}$ = 13 TeV", arXiv:1510.03068.

[17] CMS Collaboration, "Evidence for collectivity in pp collisions at the LHC", *Phys. Lett. B* **765** (2017) 193, doi:10.1016/j.physletb.2016.12.009, arXiv:1606.06198.

[18] ATLAS Collaboration, "Measurement of azimuthal anisotropy of muons from charm and bottom hadrons in $pp$ collisions at $\sqrt{s} = 13$ TeV with the ATLAS detector", arXiv:1909.01650.

[19] CMS Collaboration, "Observation of long-range near-side angular correlations in proton-lead collisions at the LHC", *Phys. Lett. B* **718** (2013) 795, doi:10.1016/j.physletb.2012.11.025, arXiv:1210.5482.

[20] ALICE Collaboration, "Long-range angular correlations on the near and away side in pPb collisions at $\sqrt{s_{NN}}$ = 5.02 TeV", *Phys. Lett. B* **719** (2013) 29, doi:10.1016/j.physletb.2013.01.012, arXiv:1212.2001.

[21] ATLAS Collaboration, "Observation of associated near-side and away-side long-range correlations in $\sqrt{s_{NN}} = 5.02$ TeV proton-lead collisions with the ATLAS detector", *Phys. Rev. Lett.* **110** (2013) 182302, doi:10.1103/PhysRevLett.110.182302, arXiv:1212.5198.

[22] LHCb Collaboration, "Measurements of long-range near-side angular correlations in $\sqrt{s_{\rm NN}} = 5$TeV proton-lead collisions in the forward region", *Phys. Lett.* **B762** (2016) 473–483, doi:10.1016/j.physletb.2016.09.064, arXiv:1512.00439.

[23] ALICE Collaboration, "Long-range angular correlations of pi, K and p in p–Pb collisions at $\sqrt{s_{_{NN}}} = 5.02$ TeV", *Phys. Lett. B* **726** (2013) 164, doi:10.1016/j.physletb.2013.08.024, arXiv:1307.3237.

[24] CMS Collaboration, "Long-range two-particle correlations of strange hadrons with charged particles in pPb and PbPb collisions at LHC energies", *Phys. Lett. B* **742** (2015) 200, doi:10.1016/j.physletb.2015.01.034, arXiv:1409.3392.

[25] CMS Collaboration, "Evidence for collective multi-particle correlations in pPb collisions", *Phys. Rev. Lett.* **115** (2015) 012301, doi:10.1103/PhysRevLett.115.012301, arXiv:1502.05382.

[26] ATLAS Collaboration, "Measurement of multi-particle azimuthal correlations in $pp$, $p$+Pb and low-multiplicity Pb+Pb collisions with the ATLAS detector", *Eur. Phys. J. C* **77** (2017) 428, doi:10.1140/epjc/s10052-017-4988-1, arXiv:1705.04176.

[27] ATLAS Collaboration, "Measurement of long-range multiparticle azimuthal correlations with the subevent cumulant method in $pp$ and $p + Pb$ collisions with the ATLAS detector at the CERN Large Hadron Collider", *Phys. Rev.* **C97** (2018), no. 2, 024904, doi:10.1103/PhysRevC.97.024904, arXiv:1708.03559.

[28] PHENIX Collaboration, "Creation of quark-gluon plasma droplets with three distinct geometries", *Nature Phys.* **15** (2019) 214, doi:10.1038/s41567-018-0360-0, arXiv:1805.02973.

[29] STAR Collaboration, "Long-range pseudorapidity dihadron correlations in $d$+Au collisions at $\sqrt{s_{\rm NN}} = 200$ GeV", *Phys. Lett.* **B747** (2015) 265–271, doi:10.1016/j.physletb.2015.05.075, arXiv:1502.07652.

[30] PHENIX Collaboration, "Measurements of elliptic and triangular flow in high-multiplicity $^3$He+Au collisions at $\sqrt{s_{_{NN}}} = 200$ GeV", *Phys. Rev. Lett.* **115** (2015) 142301, doi:10.1103/PhysRevLett.115.142301, arXiv:1507.06273.

[31] PHENIX Collaboration, "Measurements of Multiparticle Correlations in $d + $ Au Collisions at 200, 62.4, 39, and 19.6 GeV and $p + $ Au Collisions at 200 GeV and Implications for Collective Behavior", *Phys. Rev. Lett.* **120** (2018), no. 6, 062302, doi:10.1103/PhysRevLett.120.062302, arXiv:1707.06108.

[32] A. Badea et al., "Measurements of two-particle correlations in $e^+e^-$ collisions at 91 GeV with ALEPH archived data", *Submitted to Phys. Rev. Lett* (2019) arXiv:1906.00489.

[33] J. L. Nagle and W. A. Zajc, "Small System Collectivity in Relativistic Hadronic and Nuclear Collisions", *Ann. Rev. Nucl. Part. Sci.* **68** (2018) 211, doi:10.1146/annurev-nucl-101916-123209, arXiv:1801.03477.

[34] S. Voloshin and Y. Zhang, "Flow study in relativistic nuclear collisions by Fourier expansion of azimuthal particle distributions", *Z. Phys. C* **70** (1996) 665, doi:10.1007/s002880050141, arXiv:hep-ph/9407282.

[35] B. H. Alver, C. Gombeaud, M. Luzum, and J.-Y. Ollitrault, "Triangular flow in hydrodynamics and transport theory", *Phys. Rev. C* **82** (2010) 034913, doi:10.1103/PhysRevC.82.034913, arXiv:1007.5469.

[36] B. Schenke, S. Jeon, and C. Gale, "Elliptic and triangular flow in event-by-event D=3+1 viscous hydrodynamics", *Phys. Rev. Lett.* **106** (2011) 042301, doi:10.1103/PhysRevLett.106.042301, arXiv:1009.3244.

[37] Z. Qiu, C. Shen, and U. Heinz, "Hydrodynamic elliptic and triangular flow in Pb-Pb collisions at $\sqrt{s_{_{NN}}}$ = 2.76 TeV", *Phys. Lett. B* **707** (2012) 151, doi:10.1016/j.physletb.2011.12.041, arXiv:1110.3033.

[38] B. Alver and G. Roland, "Collision geometry fluctuations and triangular flow in heavy-ion collisions", *Phys. Rev. C* **81** (2010) 054905, doi:10.1103/PhysRevC.82.039903, 10.1103/PhysRevC.81.054905, arXiv:1003.0194.

[39] K. Dusling, W. Li, and B. Schenke, "Novel collective phenomena in high-energy proton-proton and proton-nucleus collisions", *Int. J. Mod. Phys.* **E25** (2016), no. 01, 1630002, doi:10.1142/S0218301316300022, arXiv:1509.07939.

[40] A. Andronic et al., "Heavy-flavour and quarkonium production in the LHC era: from proton-proton to heavy-ion collisions", *Eur. Phys. J. C* **76** (2016) 107, doi:10.1140/epjc/s10052-015-3819-5, arXiv:1506.03981.

[41] X. Dong, Y.-J. Lee, and R. Rapp, "Open Heavy-Flavor Production in Heavy-Ion Collisions", *submitted to Annu. Rev. of Nucl. and Part. Sci.* (2019) arXiv:1903.07709.

[42] STAR Collaboration, "Measurement of $D^0$ Azimuthal Anisotropy at Midrapidity in Au + Au Collisions at $\sqrt{s_{_{NN}}} = 200$ GeV", *Phys. Rev. Lett.* **118** (2017) 212301, doi:10.1103/PhysRevLett.118.212301, arXiv:1701.06060.

[43] ALICE Collaboration, "Azimuthal anisotropy of D meson production in Pb-Pb collisions at $\sqrt{s_{_{NN}}} = 2.76$ TeV", *Phys. Rev. C* **90** (2014) 034904, doi:10.1103/PhysRevC.90.034904, arXiv:1405.2001.

[44] ALICE Collaboration, "*D*-meson azimuthal anisotropy in midcentral Pb-Pb collisions at $\sqrt{\mathbf{s}_{\mathrm{NN}}} = \mathbf{5.02}$ TeV", *Phys. Rev. Lett.* **120** (2018), no. 10, 102301, doi:10.1103/PhysRevLett.120.102301, arXiv:1707.01005.

[45] CMS Collaboration, "Measurement of prompt $D^0$ meson azimuthal anisotropy in Pb-Pb collisions at $\sqrt{s_{NN}}$ = 5.02 TeV", *Phys. Rev. Lett.* **120** (2018), no. 20, 202301, doi:10.1103/PhysRevLett.120.202301, arXiv:1708.03497.

[46] ALICE Collaboration, "J/$\psi$ elliptic flow in Pb-Pb collisions at $\sqrt{s_{\mathrm{NN}}} = 5.02$ TeV", *Phys. Rev. Lett.* **119** (2017) 242301, doi:10.1103/PhysRevLett.119.242301, arXiv:1709.05260.

[47] CMS Collaboration, "Suppression and azimuthal anisotropy of prompt and nonprompt J/$\psi$ production in PbPb collisions at $\sqrt{s_{_{\mathrm{NN}}}} = 2.76$ TeV", *Eur. Phys. J.* **C77** (2017), no. 4, 252, doi:10.1140/epjc/s10052-017-4781-1, arXiv:1610.00613.

[48] CMS Collaboration, "Elliptic flow of charm and strange hadrons in high-multiplicity pPb collisions at $\sqrt{s_{_{\mathrm{NN}}}} = 8.16$ TeV", *Phys. Rev. Lett.* **121** (2018) 082301, doi:10.1103/PhysRevLett.121.082301, arXiv:1804.09767.

[49] ALICE Collaboration, "Search for collectivity with azimuthal J/$\psi$-hadron correlations in high multiplicity p-Pb collisions at $\sqrt{s_{\rm NN}}$ = 5.02 and 8.16 TeV", *Phys. Lett.* **B780** (2018) 7–20, doi:10.1016/j.physletb.2018.02.039, arXiv:1709.06807.

[50] CMS Collaboration, "Observation of prompt J/$\psi$ meson elliptic flow in high-multiplicity pPb collisions at $\sqrt{s_{\rm NN}} = 8.16$ TeV", *Phys. Lett. B* **791** (2019) 172, doi:10.1016/j.physletb.2019.02.018, arXiv:1810.01473.

[51] X. Du and R. Rapp, "In-Medium Charmonium Production in Proton-Nucleus Collisions", *JHEP* **03** (2019) 015, doi:10.1007/JHEP03(2019)015, arXiv:1808.10014.

[52] C. Zhang et al., "Elliptic Flow of Heavy Quarkonia in $pA$ Collisions", *Phys. Rev. Lett.* **122** (2019) 172302, doi:10.1103/PhysRevLett.122.172302, arXiv:1901.10320.

[53] CMS Collaboration, "Description and performance of track and primary-vertex reconstruction with the CMS tracker", *JINST* **9** (2014) P10009, doi:10.1088/1748-0221/9/10/P10009, arXiv:1405.6569.

[54] CMS Collaboration, "The CMS experiment at the CERN LHC", *JINST* **3** (2008) S08004, doi:10.1088/1748-0221/3/08/S08004.

[55] CMS Collaboration, "CMS luminosity measurement using 2016 proton-nucleus collisions at nucleon-nucleon center-of-mass energy of 8.16 TeV",.

[56] CMS Collaboration Collaboration, "CMS luminosity measurement for the 2017 data-taking period at $\sqrt{s} = 13$ TeV", Technical Report CMS-PAS-LUM-17-004, CERN, Geneva, 2018.

[57] CMS Collaboration Collaboration, "CMS luminosity measurement for the 2018 data-taking period at $\sqrt{s} = 13$ TeV", Technical Report CMS-PAS-LUM-18-002, CERN, Geneva, 2019.

[58] CMS Collaboration, "Constraints on the chiral magnetic effect using charge-dependent azimuthal correlations in $p$Pb and PbPb collisions at the CERN Large Hadron Collider", *Phys. Rev.* **C97** (2018), no. 4, 044912, doi:10.1103/PhysRevC.97.044912, arXiv:1708.01602.

[59] CMS Collaboration, "Observation of correlated azimuthal anisotropy fourier harmonics in pp and p+Pb collisions at the LHC", *Phys. Rev. Lett.* **120** (2018) 092301, doi:10.1103/PhysRevLett.120.092301, arXiv:1709.09189.

[60] H. Voss, A. Höcker, J. Stelzer, and F. Tegenfeldt, "TMVA – the toolkit for multivariate data analysis", in *XIth International Workshop on Advanced Computing and Analysis Techniques in Physics Research (ACAT)*, p. 40. 2009. arXiv:physics/0703039.

[61] T. Sjostrand, S. Mrenna, and P. Z. Skands, "A Brief Introduction to PYTHIA 8.1", *Comput. Phys. Commun.* **178** (2008) 852, doi:10.1016/j.cpc.2008.01.036, arXiv:0710.3820.

[62] CMS Collaboration, "Event generator tunes obtained from underlying event and multiparton scattering measurements", *Eur. Phys. J. C* **76** (2016) doi:10.1140/epjc/s10052-016-3988-x, arXiv:1512.00815.

[63] T. Pierog et al., "EPOS LHC: Test of collective hadronization with data measured at the CERN Large Hadron Collider", *Phys. Rev. C* **92** (2015) 034906, doi:10.1103/PhysRevC.92.034906, arXiv:1306.0121.

[64] CMS Collaboration, "Multiplicity and transverse momentum dependence of two- and four-particle correlations in pPb and PbPb collisions", *Phys. Lett. B* **724** (2013) 213, doi:10.1016/j.physletb.2013.06.028, arXiv:1305.0609.

[65] M. Nahrgang et al., "Elliptic and triangular flow of heavy flavor in heavy-ion collisions", *Phys. Rev. C* **91** (2015) 014904, doi:10.1103/PhysRevC.91.014904, arXiv:1410.5396.

[66] M. He, R. J. Fries, and R. Rapp, "Heavy flavor at the Large Hadron Collider in a strong coupling approach", *Phys. Lett. B* **735** (2014) 445, doi:10.1016/j.physletb.2014.05.050, arXiv:1401.3817.

[67] J. Xu, J. Liao, and M. Gyulassy, "Bridging soft-hard transport properties of quark-gluon plasmas with CUJET3.0", *JHEP* **02** (2016) 169, doi:10.1007/JHEP02(2016)169, arXiv:1508.00552.